Subchondral bone density and cartilage degeneration patterns in osteoarthritic metacarpal condyles of horses

Benjamin D. Young, DVM, MS; Valerie F. Samii, DVM; John S. Mattoon, DVM; Steven E. Weisbrode, VMD, PhD; Alicia L. Bertone, DVM, PhD

Objective—To evaluate and correlate patterns of subchondral bone density and articular cartilage degeneration (derived by use of gross, histologic, and computed tomographic [CT] examinations) in equine third metacarpal condyles with and without osteoarthritis.

Sample Population—8 metacarpophalangeal (MCP) joints (n = 4 horses) without osteoarthritis and 6 osteoarthritis-affected MCP joints (4).

Procedures—Horses were euthanized. The third metacarpal condyles of the joints were examined grossly and via CT (3 slice images/condyle). For 6 condylar zones, mean bone density and pattern of density distribution were determined. Data for osteoarthritis-affected and control joints were compared. Histomorphometric point count analyses identified areas of bone density for comparison with CT density measurements.

Results—Osteoarthritis-affected condyles had heterogeneous subchondral bone with focal resorptive lesions and patterned sclerosis, whereas control condyles had symmetric bone density distribution. In osteoarthritis-affected condyles, bone density determined via gray scale image density analysis was greater (dorsal and medial pattern), compared with control condyles, and differed among zones because of resorption and sclerosis. With regard to bone density in osteoarthritis-affected condyles, histologic findings correlated with CT images, and bone lesions were significantly correlated with cartilage lesions.

Conclusions and Clinical Relevance—In horses, heterogeneous distribution and greater subchondral bone density were characteristic of osteoarthritis-affected condyles, compared with control condyles. Subchondral bone lesions correlated with overlying cartilage lesions in osteoarthritis-affected MCP joints. Identification of CT image characteristics appears to predict the presence of a cartilage lesion in MCP joints of horses with osteoarthritis. (*Am J Vet Res* 2007;68:841–849)

The MCP joint has the greatest number of traumatic and degenerative lesions of appendicular joints in horses.[1,2] Because of the unique anatomic configuration, high range of motion, and small surface area of the MCP joint, the dorsal and palmar surfaces receive increasing compression as the joint is extended.[1,3,4] With increased racing speed, stress to the palmar surface of the metacarpal condyle has been calculated to be more than twice that applied to the dorsal surface.[5] Cyclic loading and strain result in a number of adaptive changes and characteristic lesions in the MCP joint, with a predilection for the palmar aspect of the metacarpal condyle.[3,5-8] Mild forms of exercise-induced remodeling can cause subchondral bone sclerosis and nonprogressive vertical splits in articular cartilage without clinical lameness. More severe conditions are often classified as traumatic lesions of racehorses.[1-3,7,9-12] Both degenerative joint disease and joint failure can result from excessive mechanical forces applied to a joint.[7,13] Early damage to the MCP joint is reversible, whereas damage progression can lead to more severe conditions including so-called traumatic osteochondrosis, osteoarthritis, or even catastrophic failure of the joint such as condylar fractures.[6,7,14-18]

Osteoarthritis can be secondary to sudden or repetitive trauma, osteochondrosis, and joint infection or instability.[1,3,19,20] The common characteristic end points in affected joints are irreversible damage to the articular cartilage, subchondral bone remodeling, thickening

Abbreviations

MCP	Metacarpophalangeal
CT	Computed tomography
HU	Hounsfield unit
PPED	Dipotassium phosphate–equivalent density

Received August 23, 2006.
Accepted January 3, 2007.
From the Comparative Orthopedic Research Laboratories, Departments of Veterinary Clinical Sciences (Young, Samii, Mattoon, Bertone) and Veterinary BioSciences (Weisbrode), College of Veterinary Medicine, The Ohio State University, Columbus, OH 43210. Dr. Young's present address is Texas Veterinary Medical Center, Department of Large Animal Clinical Sciences, College of Veterinary Medicine and Biomedical Sciences, Texas A&M University, College Station, TX 77843-4475.
Supported by The Ohio State University Council for Research Equine Research Funds.
The authors thank Amy Lehman and Amanda Johnson for statistical and technical support, respectively.
Address correspondence to Dr. Bertone.

of periarticular tissues, decreased range of motion, and joint pain.[1,19,21] Subchondral bone modeling and remodeling have been identified as crucial components in the pathogenesis of exercise-induced lesions and osteoarthritis in horses.[22-24] There is increasing evidence to suggest that the pathogenesis of exercise-induced lesions of the third metacarpal condyle of horses results from increased bone density, interference with the subchondral bone blood supply, subchondral bone necrosis and microfracture, and collapse of overlying cartilage.[2,6,7,9,13-18,22,24,25]

Identification of cartilage loss, an early signature feature of osteoarthritis, would be advantageous, but cartilage lesions are not distinguishable in survey radiographic views.[26] Identification of osseous lesions of the palmar aspect of the third metacarpal condyle via radiography is difficult, and the technique has a low sensitivity for lesion detection.[8,11,27] Various orientations of radiographic views have been developed in an attempt to highlight this region.[27,28] With invasive techniques, there is a lack of a suitable surgical exposure to the palmar aspect of the condyle, and most of the condylar cartilage lesions are obscured even via arthroscopy.[12] Inference of cartilage damage is often made from radiographic identification of osseous changes.[29,30] Results of several studies[22,23,31,32] have indicated that there is an association between subchondral bone thickening and overlying cartilage degradation within the MCP joint; however, such a correlation has not been quantified. Newer imaging techniques may be capable of monitoring early bone changes indicative of cartilage degeneration in horses.

Computed tomography allows cross-sectional imaging of anatomic features and can provide excellent detail of osseous structures with higher contrast resolution than that achieved via radiography.[33,34] Computed tomography permits more accurate identification of variation in tissue density and may be a suitable modality for detection of changes in bone density and patterns of bone density distribution.[a] Use of a tissue-density–equivalent phantom during CT scanning provides internal reference calibration with which CT values can be standardized and improves the accuracy of tissue density determination.[35-37] Tissue densities measured in HUs are converted to PPED values, which then may be compared among CT machines. Quantitative CT (or CT osteoabsorptiometry) uses software that can quantify bone density distribution. Repeatable subchondral patterns have been reported for healthy human and canine joints.[35,38] In dogs, subchondral bone of osteoarthritic femoral heads is more dense than that of unaffected femoral heads.[39]

The purpose of the study reported here was to evaluate and correlate patterns of subchondral bone density and articular cartilage degeneration (derived by use of gross, histologic, and CT examinations) in equine third metacarpal condyles with and without osteoarthritis. It was hypothesized that, in horses, greater subchondral bone density in a characteristic pattern would be present in osteoarthritic condyles, that quantitative bone density would correlate with histologic findings, and that subchondral bone density patterns would correlate with cartilage degeneration patterns, thereby enabling generation of a profile for cartilage injury from quantitative CT images.

Materials and Methods

Horses—Horses were selected for the study if they met the inclusion criteria for either the osteoarthritis-affected or control non–osteoarthritis-affected group. Inclusion of horses in the osteoarthritis-affected group was based on criteria that have been published previously and included forelimb lameness that was exacerbated by flexion of the distal portion of the limb, an abnormally large MCP joint, and radiographic evidence of osteoarthritis of the MCP joint.[20,40] Criteria for inclusion of horses in the control group were absence of lameness; negative results of a flexion test performed on the distal portion of the forelimb; and apparently normal appearance, no abnormal findings on palpation, and absence of radiographic signs of osteoarthritis of the MCP joint. Eight MCP joints from 4 horses were included in the control group. Six MCP joints from 4 horses were included in the osteoarthritis-affected group.

Specimen collection and cartilage grading—Horses were euthanized via IV injection of a mixture of pentobarbital and phenytoin[b] (> 88 mg/kg) in accordance with guidelines set forth by The Ohio State University's Animal Care and Use Committee. The MCP joints were disarticulated, and the distal third of the third metacarpal bones were isolated from the limbs. Digital photographs[c] of the articular surface of the third metacarpal condyle were obtained at a standard camera focal distance of 15 cm. For each photograph, the articular surface was divided into 6 zones (**Figure 1**). These zones were identified as follows: zone 1, dorsomedial surface of the condyle; zone 2, palmaromedial surface of the condyle; zone 3, dorsal surface of the sagittal ridge; zone 4, palmar surface of the sagittal ridge; zone 5, dorsolateral surface of the condyle; and zone 6, palmarolateral surface of the condyle. Dorsal and palmar zones were separated by the transverse ridge of the metacarpal condyle. Two investigators (BDY and ALB), who were unaware of the group to which the joint had been assigned, individually graded the photographs with regard to articular cartilage lesions as evidenced by erosion, fibrillation, or scoring of the cartilage. A lesion was determined to be a full-thickness erosion of cartilage if the bone surface was visible. A grade for lesion extent and severity was determined for each zone. For assessments of lesion extent, grade 0 indicated no lesion; the other grades were assigned on the basis of the percentage of the zone's total area that was affected (grade 1, 1% to 25%; grade 2, 26% to 50%; grade 3, 51% to 75%; and grade 4, 76% to 100%). For assessments of cartilage lesion severity, grade 0 indicated no lesion; the other grades were assigned on the basis of the percentage of cartilage lesions in the zone that were full thickness (grade 1, 1% to 25%; grade 2, 26% to 50%; grade 3, 51% to 75%; and grade 4, 76% to 100%). For each zone, the scores from each observer were multiplied to produce a cartilage degeneration index (cartilage degeneration index was equal to lesion extent grade multiplied by lesion severity grade) and values were aver-

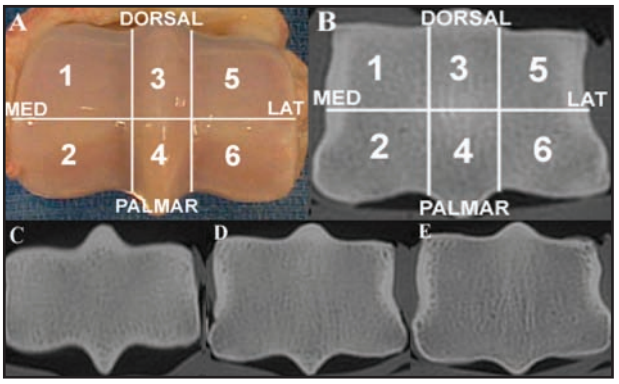

Figure 1—Representative photographic (A) and CT (B–E) images of a third metacarpal condyle without signs of osteoarthritis obtained from a horse for which lameness was not evident; results of a flexion test performed on the distal portion of the forelimb were negative; and the MCP joint had an apparently normal appearance, no abnormalities detectable via palpation, and no radiographic signs of osteoarthritis. Photographic and CT images were divided into 6 standard zones for analysis. These zones were identified as follows: zone 1, dorsomedial surface of the condyle; zone 2, palmaromedial surface of the condyle; zone 3, dorsal surface of the sagittal ridge; zone 4, palmar surface of the sagittal ridge; zone 5, dorsolateral surface of the condyle; and zone 6, palmarolateral surface of the condyle. Dorsal and palmar zones were separated by the transverse ridge of the metacarpal condyle. Three CT image slices (6 [slice 1; C], 12 [slice 2; D], and 18 [slice 3; E] mm from the most distal aspect of the joint surface) were analyzed for each metacarpal condyle

aged between the 2 observers. Intra- and interobserver variabilities were not calculated.

CT—A series of 1-mm transverse contiguous CT images of the distal 20 mm of the disarticulated third metacarpal condyle in air were obtained by use of a fourth-generation helical CT scanner[d] in a bone algorithm (130 kVp; 150 mAs; and 140-mm field of view); a dipotassium phosphate phantom[e] was included in each image. The 5 cylinders within the phantom contained 5 materials of known tissue-equivalent densities; these included dipotassium phosphate solution (200, 100, and 50 mg/mL), water, and high-density polyethylene.

CT image pattern analysis—Three image slices (6, 12, and 18 mm from the most distal aspect of the joint surface [slices 1, 2, and 3, respectively]) were analyzed for each metacarpal condyle (Figure 1) by use of 2 image analysis programs.[f,g] The images were evaluated in identical orientation (dorsal aspect at top, palmar aspect at bottom, medial aspect at left side, and lateral aspect at right side). The gray scale range of all the metacarpal condyles was determined by use of one of the image analysis programs,[f] thereby providing a total range of bone densities among all images (20- to 240-pixel gray scale values). This gray scale range was divided into 5 equal portions, with each quintile representing 20% of the total range of bone densities (ie, quintiles of 0% to 20%, 21% to 40%, 41% to 60%, 61% to 80%, and 81% to 100%). Each quintile was individually highlighted to provide visual mapping of bone within each density quintile. The number of highlighted pixels per individual quintile for each image slice was recorded. After this procedure was completed for all 5 quintiles for a CT image slice, the counts of highlighted pixels were summed and the percentage of the total number of pixels associated with the image of the metacarpal condyle that were included in a given quintile was calculated.

Slice 1, 2, and 3 images from joints in the control and osteoarthritis-affected groups were digitally summed to create 1 composite image/slice for each group by use of image analysis software.[g] These composite images were then analyzed by use of other image analysis software[f] in the same manner as each individual image slice was analyzed (ie, each density quintile was highlighted and recorded). Additionally, 2 quintiles (61% to 80% and 81% to 100%) were highlighted for the composite images and recorded, thereby creating a visual map of the most dense bone within each metacarpal condyle composite.

Mean bone density measurement by CT—The 6 zones in image slices 1 to 3 were analyzed for each metacarpal condyle by hand drawing regions of interest around each of the 6 zones of the subchondral bone. By use of CT image software,[d] mean area and bone density measurements were recorded (as square millimeters and HUs, respectively). For HU conversion, 240-mm^2 regions of interest were drawn within each of 5 tissue-equivalent cylinders of the phantom, and mean HU values were recorded. Hounsfield unit values were then converted to PPED values by use of a regression equation according to a previously described method.[35]

Bone lesion grades—Each zone within image slices 1, 2, and 3 was examined and assigned 2 grades for the extent of bone sclerosis and bone resorption by each of 3 investigators (BDY, JSM, and VFS). For assessments of either bone sclerosis or bone resorption, grade 0 indicated no lesion; the other grades were assigned on the basis of the percentage of the zone's total area that was affected (grade 1, 1% to 25%; grade 2, 26% to 50%; grade 3, 51% to 75%; and grade 4, 76% to 100%). A third grade was assigned for the severity of any sclerotic lesions present within the subchondral trabecular bone as follows: grade 0, no lesion; grade 1, minimal (ie, slightly distinguishable increase in density, compared with findings in clinically normal joints); grade 2, mild (easily distinguishable increase in bone density); grade 3, moderate (dramatic increase in bone density that was still less dense than cortical bone in the subchondral bone plate); and grade 4, severe (indistinguishable from cortical bone in the subchondral bone plate). The 3 bone lesion grades were summed to produce a bone lesion index (bone lesion index was equal to sclerotic lesion extent grade multiplied by sclerotic lesion severity grade, plus the resorptive lesion extent grade). For each zone, the bone lesion indices from each slice and each observer were averaged to obtain 1 overall bone lesion index. Intra- and interobserver variabilities were not calculated.

Histologic evaluation of metacarpal condyles—Each metacarpal condyle was sectioned with a band saw along transverse planes corresponding to the same level of the analyzed CT images (at 6, 12, and 18 mm from the most distal aspect of the joint surface) and stored at –70°C. Sections (10 µm) of each portion of the condyle section were obtained by use of a tissue cutting and grinding system[h] and stained with Masson trichrome.

Areas of increased subchondral bone density and focal resorptive lesions evident on CT images were identified on the tissue sections and examined microscopically at 40× and 100× magnification by 2 investigators (BDY and SEW). The composition of bone within these lesions was characterized.

Twenty sites from the CT images were selected for histomorphometric point-count analysis; 10 sites were identified as areas of increased density, and 10 sites were identified as areas of apparently normal bone density. Within each site, fields of 18 mm^2 were examined at 2× magnification by use of a calibrated, orthogonal, 100-point lens grid. Points overlying bone and points overlying nonbone structures (vascular or marrow spaces) were counted separately. Counts were made within each site until 100 bone counts had been attained. The resulting data yielded a ratio of bone to nonbone composition for each site.

Statistical analysis—The simple Pearson correlation between the cartilage degeneration index and bone lesion index was calculated. A mixed-effects model was applied to these data with bone lesion index as the outcome and cartilage degeneration index as the main predictor, along with the group and zone of the measurement as covariates.[41] The estimated change in bone lesion index per unit increase in cartilage degeneration index was then estimated from the model for each zone.

For each slice, the percentage of bone in the 3 quintiles from 41% through 100% was calculated, as well as the percentage of bone in the 2 quintiles from 61% through 100%. Then, linear mixed-effects models were applied to the data with the percentage of bone in the 3 quintiles from 41% through 100% as the outcome and the group, slice, and side (left or right) as the main covariates of interest. From the model, the mean difference (with 95% confidence intervals) in percentage of bone between the osteoarthritis-affected and control groups for each slice was calculated.

Mean density measurements were first summarized within each zone and slice for joints in both the osteoarthritis-affected and control groups. Linear mixed-effects models were applied to the data to account for the various correlations between measurements within a particular horse. The outcome was bone density, and the fixed effects were group (osteoarthritis-affected or control), slice, side (left or right), and zone; the intercept was considered a random effect. Spatial correlation structuring was applied so that the correlation between any 2 density measurements within a joint was related to the physical distance between them, as determined by their zones and slices. The presence of significant 2-way interactions between group and all other factors in the model was investigated. Model estimates were provided for group differences of interest, and 95% confidence intervals were calculated. Similar models were used to compare bone density between slices and zones within the osteoarthritis-affected group. A significance level of $\alpha = 0.003$ (Bonferroni) was used to account for multiple comparisons.

The ratio of bone to nonbone composition for 6 joints with both apparently normal and sclerotic areas was compared by use of the nonparametric Wilcoxon signed rank test. Next, an ANCOVA was used to compare the ratio between those normal and sclerotic areas, with horse and side as covariates. The estimated difference (along with 95% confidence interval) in ratios was calculated. All analyses were performed by use of computer software.[i] For all assessments, a value of $P < 0.05$ was considered significant.

Results

Cartilage and bone lesion indices—A significant ($P < 0.001$) positive correlation ($r = 0.404$) was identified between the severity of subchondral bone lesions determined via CT images and articular cartilage lesions determined grossly. Cartilage degeneration indices were greater ($P < 0.001$) in palmar zones, compared with dorsal zones, and greater ($P < 0.001$) in osteoarthritis-affected condyles, compared with control condyles (**Table 1**; **Figure 2**). Bone lesion indices were greater ($P < 0.001$) in osteoarthritis-affected condyles, compared with control condyles, for zones 1, 2, 4, and 6. Within the osteoarthritis-affected condyles, bone lesion indices were greatest in zones 1 and 2 (medial aspects) and least in zones 3 and 4 (sagittal ridge).

Evaluation of CT images—Subjective evaluation of CT images revealed that the subchondral bone in control joints was typically homogeneous and symmetric in density (Figure 2). The subchondral bone plate was easily distinguished from trabecular bone in all areas of the con-

Table 1—Mean ± SD cartilage degeneration and bone lesion indices determined for 6 osteoarthritis-affected and 8 unaffected control metacarpal condyles obtained from MCP joints of horses with (n = 4) and without (4) clinical signs of osteoarthritis.

Index	Group (No. of joints)	Condylar zone 1	2	3	4	5	6
Cartilage degeneration	Control (8)	0 ± 0.0	0 ± 0.0	0 ± 0.0	0.1 ± 0.4	0 ± 0.0	0 ± 0.0
	Affected (6)	0.9 ± 0.5[a]	9 ± 4.1*[b]	0.5 ± 0.6[a]	4.4 ± 4.9*[c]	0.6 ± 0.7[a]	5 ± 2.1*[c]
Bone lesion	Control (8)	2.9 ± 1.4	1.7 ± 1.2	2.9 ± 0.7	0.8 ± 0.8	2.7 ± 1.1	1.5 ± 0.8
	Affected (6)	6.9 ± 2.8†[d]	7.1 ± 1.6†[d]	3 ± 2.6[e]	2.9 ± 1.1†[e]	4.6 ± 3.7[f]	4.6 ± 3.1†[f]

*Cartilage degeneration index significantly ($P < 0.001$) different from that of the control group for this zone. †Bone lesion index significantly ($P = 0.002$) different from that of the control group for this zone.
[a-c]Within the osteoarthritis-affected group, values of cartilage degeneration index with different superscript letters are significantly ($P < 0.001$) different. [d-f]Within the osteoarthritis-affected group, values of bone lesion index with different superscript letters are significantly ($P = 0.01$) different.

dyle. Subtle trabecular sclerosis was present occasionally.

Focal resorptive lesions and severe subchondral bone sclerosis were only detected in osteoarthritis-affected condyles. Sclerosis was more predominant in the medial aspect of osteoarthritis-affected condyles. In some areas, the trabecular bone was as dense as the subchondral bone plate, making the 2 indistinguishable. Resorptive lesions were always palmar in location and most often palmaromedial.

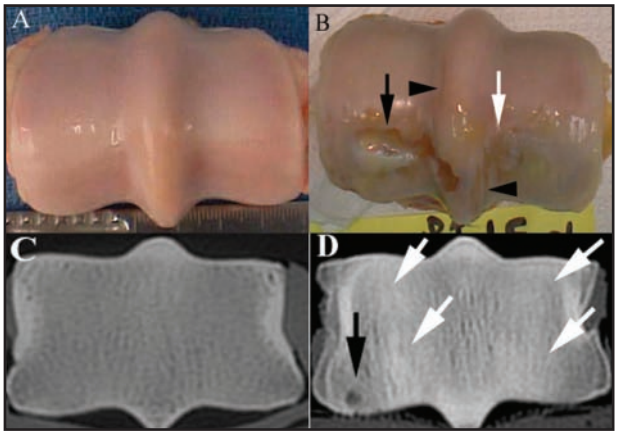

Figure 2—Photographic and CT images of third metacarpal condyles obtained from horses without (control group) and with osteoarthritis of the MCP joint. A—Photograph of a nonosteoarthritis-affected metacarpal condyle. Notice the absence of any cartilage lesions. B—Photograph of an osteoarthritis-affected condyle. Notice the full-thickness cartilage lesion in zone 2 (black arrow) extending to zone 4. A smaller partial-thickness cartilage lesion (white arrow) and linear scoring (black arrowheads), which are typical features of osteoarthritis-affected condyles, are also visible. C—Computed tomographic image of a control metacarpal condyle. No cartilage lesions are detectable. D—Computed tomographic image (slice 2) of an osteoarthritis-affected condyle. Notice the focal resorptive lesion in zone 2 (black arrow) and sclerotic lesions in zones 1, 2, 5, and 6 (white arrows). *See* Figure 1 for key.

Image analysis of CT images (gray scale)—The trabecular bone of the control condyles was almost exclusively assigned to the 21% to 40% density quintile, whereas the cortical bone was nearly uniformly assigned to the 41% to 60% density quintile (**Figure 3**). In contrast, trabecular and cortical bone of osteoarthritis-affected condyles was assigned to several density quintiles (**Figure 4**). The percentage of each condyle highlighted from 41% to 100% of the gray scale range was greater in osteoarthritis-affected condyles, compared with control condyles for slices 2 and 3 ($P = 0.031$ and $P = 0.003$, respectively). The percentage of each condyle highlighted from 61% to 100% of the gray scale range was significantly higher in osteoarthritis-affected condyles, compared with the control condyles, for slices 1, 2, and 3 ($P = 0.002$, $P = 0.001$, and $P = 0.023$, respectively). The percentage of each condyle highlighted from 81% to 100% of the gray scale range was greater in osteoarthritis-affected condyles, compared with control condyles, for slice 2 ($P = 0.034$).

Mean PPED analysis of CT—There were no significant differences in mean metacarpal condyle bone density PPED values between osteoarthritis-affected condyles and control condyles by slice (**Table 2**). Com-

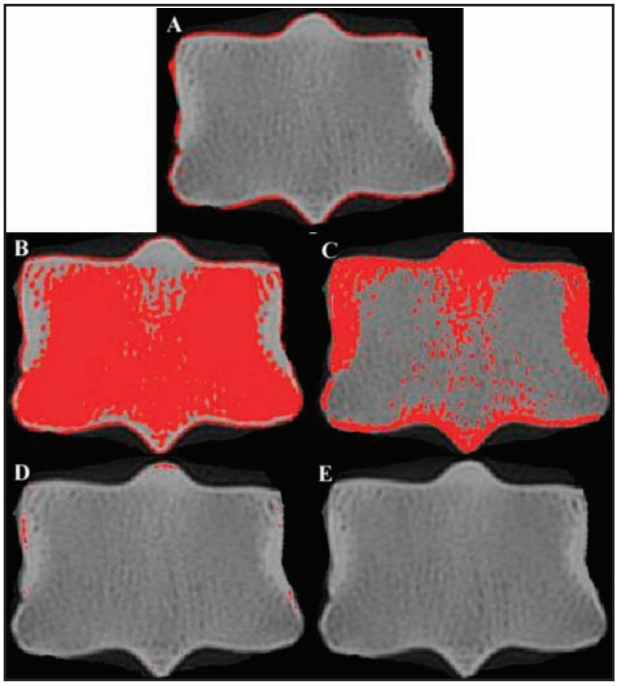

Figure 3—Results of gray scale image analysis of slice 3 CT images of a typical control metacarpal condyle from a horse without osteoarthritis. Highlighted areas are indicative of bone density that was assigned to density range quintiles of 0% to 20% (A), 21% to 40% (B), 41% to 60% (C), 61% to 80% (D), and 81% to 100% (E). There was uniform enhancement of trabecular bone almost exclusively in the 20% to 40% density quintile. Cortical bone was highlighted almost exclusively in the 60% to 80% density quintile. *See* Figure 1 for key.

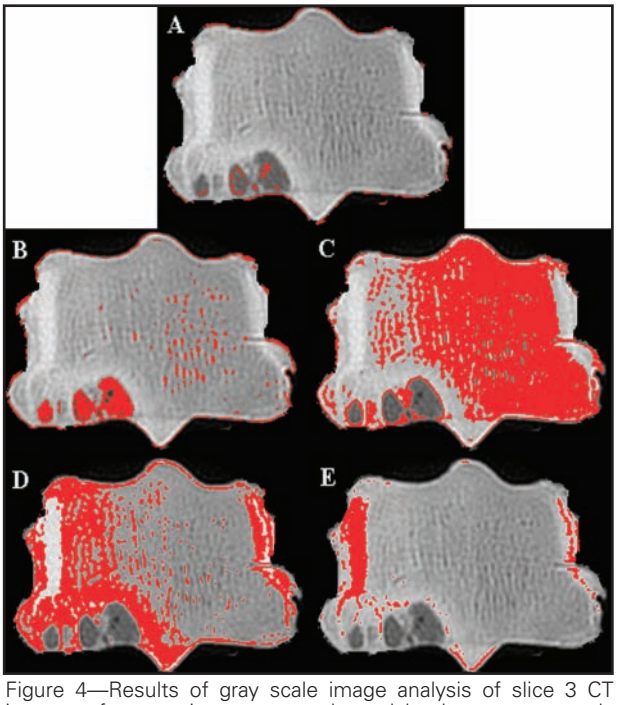

Figure 4—Results of gray scale image analysis of slice 3 CT images of an equine metacarpal condyle that was severely affected by osteoarthritis. Highlighted areas are indicative of bone density that was assigned to density range quintiles of 0% to 20% (A), 21% to 40% (B), 41% to 60% (C), 61% to 80% (D), and 81% to 100% (E). Severe resorptive lesions are present in the palmaromedial aspect of the condyle. Trabecular bone was heterogeneous and appeared highlighted for all bone density quintiles. Sclerotic bone surrounded the resorptive lesions and was preferentially distributed medially. *See* Figure 1 for key.

Table 2—Mean ± SD PPED values determined from 3 CT images (6 [slice 1], 12 [slice 2], and 18 [slice 3] mm from the most distal aspect of the joint surface) for 6 osteoarthritis-affected and 8 unaffected control metacarpal condyles obtained from MCP joints of horses with (n = 4) and without (4) clinical signs of osteoarthritis.

	Condylar zone						
Group	**1**	**2**	**3**	**4**	**5**	**6**	**Mean slice value**
Control							
Slice 1	875 ± 96.7	817 ± 113.3	783 ± 72.1	754 ± 70.8	881 ± 91.8	850 ± 105.2	829 ± 85.9
Slice 2	842 ± 76.2	717 ± 86.0	822 ± 36.9	697 ± 36.0	810 ± 87.8	745 ± 95.9	765 ± 74.3
Slice 3	777 ± 78.8	630 ± 65.2	738 ± 43.6	620 ± 37.6	759 ± 83.0	647 ± 80.7	686 ± 62.4
Mean zone value	824 ± 82.2	705 ± 112.1	773 ± 57.8	673 ± 79.9	818 ± 86.9	730 ± 117.8	
Affected							
Slice 1	882 ± 93.5	784 ± 146.3	762 ± 86.5	780 ± 87.9	754 ± 112.7	729 ± 106.0	783 ± 63.8
Slice 2	878 ± 102.1	831 ± 37.5	770 ± 109.4	755 ± 108.8	761 ± 132.5	718 ± 121.8	793 ± 57.3
Slice 3	822 ± 88.5	714 ± 44.6	669 ± 79.2	638 ± 52.5	689 ± 126.1	626 ± 100.2	698 ± 47.7
Mean zone value	861 ± 93.5[a]	777 ± 98.6[b]	734 ± 98.9[b]	725 ± 103.2[b]	735 ± 121.1*[b]	691 ± 113.5[c]	

*Mean value significantly ($P < 0.05$) less than mean value for control group.
[a-c]Within the osteoarthritis-affected group, zone values with different superscript letters are significantly ($P < 0.001$) different.

pared with control condyles, the composite mean PPED and mean PPED values among slices, sides (ie, right vs left limb), or zones ($P = 0.9$) in osteoarthritis-affected condyles did not differ. Although zone 2 (palmaromedial) appeared to be more dense in osteoarthritis-affected condyles, compared with control condyles, this difference was not significant ($P = 0.06$); however, zone 5 (dorsolateral) in osteoarthritis-affected condyles was significantly ($P = 0.05$) less dense than the equivalent zone in control condyles.

In osteoarthritis-affected condyles, slice 1 (distal) was more dense ($P < 0.001$) than slice 2 or 3, zone 1 (dorsomedial) was more dense ($P < 0.001$) than all other zones, and zone 2 (palmaromedial) was more dense ($P < 0.001$) than zone 6 (palmarolateral). A gradation of bone density from the most dense zone (dorsomedial; zone 1) to the least dense zone (palmarolateral; zone 6) was detected within both osteoarthritis-affected and control condyles. The ratio of mean bone density in zone 1 to that in zone 6 in osteoarthritis-affected condyles appeared to be greater than the finding in control condyles, but this difference was not significant ($P = 0.08$); nevertheless, it is possible that there is greater heterogeneity of bone density in osteoarthritis-affected condyles **(Figure 5)**.

Histomorphometric analysis—The ratio of bone to nonbone composition was significantly ($P < 0.001$) greater in areas that had high bone density on CT images (mean ratio, 3.57), compared with the ratio for areas of what was considered normal bone density (mean ratio, 0.96). The effects of horse and side (ie, right vs left limb) did not affect the significance of this difference. In osteoarthritis-affected joints, areas of increased bone density identified via CT were characterized histologically by increased compact lamellar osteonal and lamellar nonosteonal bone. The marrow spaces were greatly reduced in size, compared with apparently normal regions of bone.

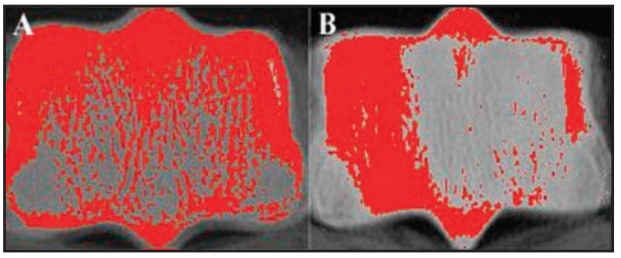

Figure 5—Composite slice 3 CT images of control (A) and osteoarthritis-affected (B) metacarpal condyles obtained from 4 horses in each group in which areas of most dense bone (ie, 60% to 100% of the gray scale range of bone density) are highlighted. The composite image of the control condyles reveals uniform distribution of bone density, whereas the composite image of the osteoarthritis-affected condyles reveals heterogeneous bone density with medial distribution of the most dense bone. *See* Figure 1 for key.

Discussion

Results of the present study have confirmed and quantified different patterns of subchondral bone density of the third metacarpal condyles of horses with clinical evidence of osteoarthritis, compared with findings in nonosteoarthritis-affected condyles. Marked heterogeneity of subchondral bone density was a distinguishing feature of osteoarthritis. Focal resorptive lesions and severe subchondral bone sclerosis were detected only in osteoarthritis-affected metacarpal condyles. In an affected metacarpal condyle, sclerosis was more prominent in the medial aspect and resorptive lesions were always in the palmar region and most often in the palmaromedial aspect.

Use of image analysis software confirmed a relatively narrow range and homogeneous distribution of bone density in equine metacarpal condyles without osteoarthritis. Consequently, the trabecular bone was assigned to the 21% to 40% quintile of the total gray scale range. In contrast, there was a more heterogeneous distribution of subchondral bone and a greater range of bone densities in osteoarthritis-affected condyles, as evidenced by a wider gray scale range. Quantitative measurements of mean bone density revealed a medial distribution of sclerosis within osteoarthritis-affected condyles; the most dense bone was located in the dorsomedial zone of the condyles. The palmaromedial zone was significantly more dense than the palmarolateral zone despite a greater number of palmaromedial resorptive lesions. This finding may be explained by severe sclerosis of the palmaromedial aspect of those osteoarthritis-affected condyles without resorptive lesions, as well as by severe sclerosis surrounding the re-

sorptive lesions when present. This heterogeneity was identified visually and quantified through the image gray scale method of analysis. Osteoarthritis-affected condyles had a significantly greater percentage of high-density bone (assigned within the 61% to 80% and 81% to 100% quintiles of the gray scale range) than control condyles. Within resorptive lesions, which were detected in only the osteoarthritis-affected condyles, bone was assigned to the lowest density range (ie, the 0% to 20% quintile) of the gray scale range. In comparison, only small foci of marrow spaces and vascular canals were highlighted and assigned to the lowest quintile in control condyles. Composite CT images were generated to enhance common areas of increased bone density or resorption and eliminate the effects of randomly distributed lesions. The medial distribution of sclerosis in osteoarthritis-affected condyles was clearly visible on the composite images.

One previous study[5] of bone density in third metacarpal subchondral bone of horses involved evaluation of condyles primarily from Thoroughbreds of various ages that were undergoing race training and from 2 juvenile horses with no training history. The primary conclusion based on densitometric measurements of microradiographic views was that the most dense bone was distributed along the palmar aspect of the condyle; from subjective evaluation of CT images, the investigators concluded that the "lateral [aspect of the] condyle usually appeared more dense than the medial."[5] Several other studies[9,42-44] have revealed that the palmar aspect of the condyle is more dense than the dorsal aspect. In the present study, the quantitative and pattern analyses of osteoarthritis-affected condyles revealed a dorsal and medial distribution of the most dense bone. Thus, evaluation of specific patterns of subchondral bone density may represent a means by which osteoarthritic and nonosteoarthritis-affected condyles in horses can be distinguished.

In our study, greater bone density and heterogeneity of density distribution in osteoarthritic condyles, compared with nonosteoarthritic condyles from clinically unaffected horses, were more readily identified by use of a gray scale assessment of bone density than by PPED assessment. This likely represented the limitations of the software used to measure mean density over a defined area. For purposes of the study, we defined condylar zones for analysis, rather than outline regions of interest around individual lesions, because the intent was to objectively identify and characterize osteoarthritis in the condyles via CT. Outlining regions of interest around lesions would likely have distinguished lesions from unaffected condyles, but would not have served to routinely predict osteoarthritis in affected condyles because lesions would have to be sufficiently developed to be clearly visible. It is possible that the use of a greater number of smaller condylar zones could have enabled bone density differences to be revealed via PPED assessment.

It is well established that reliable and accurate assessment of subchondral bone mineral content can be achieved by use of quantitative CT.[35-38,45-47] Via quantitative CT, subchondral bone density can be quantified and compared among CT image slices.[36] In the present study, we predicted that subchondral bone sclerosis in osteoarthritis-affected condyles would increase the mean condylar bone density, but this was counterbalanced by the loss of bone in focal areas. The result was an inability of simple, objective PPED measures to identify osteoarthritis in affected equine MCP joints. The gray scale imaging analysis offered several advantages over PPED assessment; by use of the former, quantitation of bone density by degree of density rather than through calculation of mean bone density successfully distinguished the patterns of increased and decreased bone density in the osteoarthritis-affected condyles. This method avoided arbitrary divisions of regions of interest and may have been less susceptible to the artificial exclusion of portions of high-density bone cortex that is associated with use of hand-drawn regions of interest. Also, the presence of low-density resorptive lesions does not affect the gray scale imaging analysis because a mean bone density value is not calculated.

The use of histologic assessments to validate CT findings has been applied in a multitude of species,[35,37,38,44-47] but to our knowledge, the present study is the first to compare histologic and CT data from osteoarthritis-affected MCP joints in horses. By matching the location of lesions in histologic sections with the location of lesions in CT images, we were able to validate that higher-density lesions detected via CT were indeed associated with morphologically thickened trabeculae and lamellar bone formation, which resulted in significantly greater ratio of bone to nonbone composition in a affected region, compared with apparently normal regions. In another study[7] involving horses, the development of subchondral bone sclerosis of the palmar aspect of the third metacarpal condyle resulted in decreased marrow surface area, which is similar to our finding.

The present study revealed that subchondral bone lesions of osteoarthritis-affected metacarpal condyles correlated with overlying cartilage lesions, which were most severe in the palmar aspect of the condyles. This finding is similar to those of many previous studies[1-3,8,9,11] of osteoarthritis in the MCP joint of horses. In contrast, cartilage lesions on the proximal articular surface of an osteoarthritis-affected proximal phalanx are typically most severe dorsally because of dorsal concentration of loading forces on this bone during extension.[1,48,49] Cartilage lesions are difficult to identify radiographically,[29] and cartilage loss was not detected radiographically in the horses in our study. The palmar metacarpal condyle is a difficult aspect of the MCP joint surface to evaluate, even with invasive methods such as arthroscopy.[11,12,27] Magnetic resonance imaging is emerging as an effective means of evaluating cartilage; however, availability of this modality for horses remains scarce and expensive.[50,51] At present, prediction of MCP cartilage damage has been based on indirect indicators of joint cartilage health, such as joint space width[52] or subchondral bone thickening.[23,31] The results of the present study have indicated that as the severity of resorptive lesions and density of the subchondral bone increased, the extent and severity of overlying articular cartilage erosive lesions increased, thereby bestowing greater confidence in the predictive value

of characteristics of CT bone images for identification of these cartilage lesions.

Our data have suggested that CT is an effective technique for identification of subchondral bone lesions in third metacarpal condyles of horses. Quantitative assessment of CT images by use of gray scale image analysis identified significant differences in bone density between osteoarthritis-affected and control metacarpal condyles. Dipotassium phosphate–equivalent density assessment was less effective in distinguishing between osteoarthritis-affected and control equine metacarpal condyles because of the heterogeneity of osteoarthritis lesions.

a. Thomas HL, Galuppo LD, Wisner ER, et al. Computed tomography for identification of early third metacarpal traumatic palmar subchondral bone lesions (abstr), in *Proceedings*. Annu Sci Meet Am Coll Vet Radiol 2004;64.
b. Beuthanasia D, Virbac, Fort Worth, Tex.
c. Elura 20 MC, Canon USA Inc, Lake Success, NY.
d. Picker PQS CT scanner, Phillips Medical Systems Inc, Bothell, Wash.
e. Dipotassium phosphate phantom, model 3T, Mindways Software Inc, San Francisco, Calif.
f. Image J, version 1.33u, National Institutes of Health, Bethesda, Md. Available at: rsb.info.nih.gov/ij/. Accessed Dec 20, 2004.
g. MIPAV, version 1.29, Center for Information Technology and National Institutes of Health, Bethesda, Md. Available at: mipav.cit.nih.gov/. Accessed Jan 5, 2005.
h. Exakt tissue cutter/grinder, Exakt Technologies Inc, Oklahoma City, Okla.
i. SAS, version 9.1, SAS Institute Inc, Cary, NC.

References

1. Pool RR. Pathologic manifestations of joint disease in the athletic horse. In: McIlwraith CW, Trotter GW, eds. Joint disease in the horse. Philadelphia: Saunders, 1996;87–104.
2. Pool RR, Meagher DM. Pathologic findings and pathogenesis of racetrack injuries. *Vet Clin North Am Equine Pract* 1990;6:1–30.
3. Pool RR. Joint disease in the athletic horse: a review of pathologic findings and pathogenesis, in *Proceedings*. 41st Annu Meet Am Assoc Equine Pract 1995;20–34.
4. Colahan P, Turner TA, Poulos P. Mechanical functions and sources of injury in the fetlock and carpus, in *Proceedings*. 33rd Annu Meet Am Assoc Equine Pract 1987;689–699.
5. Riggs CM, Whitehouse GH, Boyde A. Structural variation of the distal condyles of the third metacarpal and third metatarsal bones in the horse. *Equine Vet J* 1999;31:130–139.
6. Radtke CL, Danova NA, Scollay MC, et al. Macroscopic changes in the distal ends of the third metacarpal and metatarsal bones of Thoroughbred racehorses with condylar fractures (Erratum published in *Am J Vet Res* 2003;64:1420). *Am J Vet Res* 2003;64:1110–1116.
7. Norrdin RW, Kawcak CE, Capwell BA, et al. Subchondral bone failure in an equine model of overload arthrosis. *Bone* 1998;22:133–139.
8. O'Brien TR, Hornof WJ, Meagher DM. Radiographic detection and characterization of palmar lesions in the equine fetlock joint. *J Am Vet Med Assoc* 1981;178:231–237.
9. Hornof WJ, O'Brien TR, Pool RR. Osteochondritis dissecans of the distal metacarpus in the adult racing thoroughbred horse. *Vet Radiol Ultrasound* 1981;22:98–106.
10. Ferraro GL. Lameness diagnosis and treatment in the Thoroughbred racehorse. *Vet Clin North Am Equine Pract* 1990;6:63–84.
11. O'Brien TR. Disease of the Thoroughbred fetlock joint—a comparison of radiographic signs with gross pathologic lesions, in *Proceedings*. 23rd Annu Meet Am Assoc Equine Pract 1977;367–380.
12. Nixon AJ. Osteochondrosis and osteochondritis dissecans of the equine fetlock. *Compend Contin Educ Pract Vet* 1990;12:1463–1474.
13. Norrdin RW, Bay BK, Drews MJ, et al. Overload arthrosis: strain patterns in the equine metacarpal condyle. *J Musculoskelet Neuronal Interact* 2001;1:357–362.
14. Stepnik MW, Radtke CL, Scollay MC, et al. Scanning electron microscopic examination of third metacarpal/third metatarsal bone failure surfaces in thoroughbred racehorses with condylar fracture. *Vet Surg* 2004;33:2–10.
15. Riggs CM, Whitehouse GH, Boyde A. Pathology of the distal condyles of the third metacarpal and third metatarsal bones of the horse. *Equine Vet J* 1999;31:140–148.
16. Boyde A, Haroon Y, Jones SJ, et al. Three dimensional structure of the distal condyles of the third metacarpal bone of the horse. *Equine Vet J* 1999;31:122–129.
17. Riggs CM. Aetiopathogenesis of parasagittal fractures of the distal condyles of the third metacarpal and third metatarsal bones—review of the literature. *Equine Vet J* 1999;31:116–120.
18. Rick MC, O'Brien TR, Pool RR, et al. Condylar fractures of the third metacarpal bone and third metatarsal bone in 75 horses: radiographic features, treatments, and outcome. *J Am Vet Med Assoc* 1983;183:287–296.
19. Johnston SA. Osteoarthritis. Joint anatomy, physiology, and pathobiology. *Vet Clin North Am Small Anim Pract* 1997;27:699–723.
20. Simmons EJ, Bertone AL, Weisbrode SE. Instability-induced osteoarthritis in the metacarpophalangeal joint of horses. *Am J Vet Res* 1999;60:7–13.
21. Strand E, Martin GS, Crawford MP, et al. Intra-articular pressure, elastance and range of motion in healthy and injured racehorse metacarpophalangeal joints. *Equine Vet J* 1998;30:520–527.
22. Kawcak CE, McIlwraith CW, Norrdin RW, et al. The role of subchondral bone in joint disease: a review. *Equine Vet J* 2001;33:120–126.
23. Firth EC, Delahunt J, Wichtel JW, et al. Galloping exercise induces regional changes in bone density within the third and radial carpal bones of Thoroughbred horses. *Equine Vet J* 1999;31:111–115.
24. Reilly GC, Currey JD, Goodship AE. Exercise of young thoroughbred horses increases impact strength of the third metacarpal bone. *J Orthop Res* 1997;15:862–868.
25. Radin EL. Subchondral bone changes and cartilage damage. *Equine Vet J* 1999;31:94–95.
26. Nilsson G, Olsson SE. Radiologic and patho-anatomic changes in the distal joints and the phalanges of the standardbred horse. *Acta Vet Scand Suppl* 1973;44:1–57.
27. Pilsworth RC, Hopes R, Greet TR. A flexed dorso-palmar projection of the equine fetlock in demonstrating lesions of the distal third metacarpus. *Vet Rec* 1988;122:332–333.
28. Hornof WJ, O'Brien TR. Radiographic evaluation of the palmar aspect of the equine metacarpal condyles: a new projection. *Vet Radiol Ultrasound* 1980;21:161–167.
29. Lamb CR. Contrast radiography of equine joints, tendon sheaths, and draining tracts. *Vet Clin North Am Equine Pract* 1991;7:241–257.
30. Farrow CS. The fetlock joint. In: *Veterinary diagnostic imaging—the horse*. St Louis: Mosby, 2006;96–129.
31. Cantley CE, Firth EC, Delahunt JW, et al. Naturally occurring osteoarthritis in the metacarpophalangeal joints of wild horses. *Equine Vet J* 1999;31:73–81.
32. Walker JE, Lewis CW, MacLeay JM, et al. Assessment of subchondral bone mineral density in equine metacarpophalangeal and stifle joints. *Biomed Sci Instrum* 2004;40:272–276.
33. Curry TS III, Dowdey JE, Murry RD Jr. Computed tomography. In: *Christensen's physics of diagnostic radiology*. 4th ed. Philadelphia: Lippincott Williams & Wilkins, 1990;289–322.
34. Bushberg JT, Seibert JA, Leidholdt EM Jr, et al. Computed tomography. In: *The essential physics of medical imaging*. 2nd ed. Philadelphia: Lippincott Williams & Wilkins, 2002;327–372.
35. Samii VF, Les Clifford M, Schulz KS, et al. Computed tomographic osteoabsorptiometry of the elbow joint in clinically normal dogs. *Am J Vet Res* 2002;63:1159–1166.
36. Cann CE. Quantitative CT for determination of bone mineral density: a review. *Radiology* 1988;166:509–522.

37. Chen X, Lam YM. Technical note: CT determination of the mineral density of dry bone specimens using the dipotassium phosphate phantom. *Am J Phys Anthropol* 1997;103:557–560.
38. Muller-Gerbl M, Putz R, Kenn R. Demonstration of subchondral bone density patterns by three-dimensional CT osteoabsorptiometry as a noninvasive method for in vivo assessment of individual long-term stresses in joints. *J Bone Miner Res* 1992;7(suppl 2):S411–S418.
39. Chalmers HJ, Dykes NL, Lust G, et al. Assessment of bone mineral density of the femoral head in dogs with early osteoarthritis. *Am J Vet Res* 2006;67:796–800.
40. Smith KJ, Bertone AL, Weisbrode SE, et al. Gross, histologic, and gene expression characteristics of osteoarthritic articular cartilage of the metacarpal condyle of horses. *Am J Vet Res* 2006;67:1299–1306.
41. Brown H, Prescott R. *Applied mixed models in medicine*. New York: John Wiley & Sons, 1999.
42. Kaneko M, Kiryu K, Oikawa M, et al. Longitudinal cannon-bone fracture and subchondral osteosclerosis in the racehorse—an examination of the cannon-bones of two cases with the fracture. *Bull Equine Res Inst* 1980;17:1–7.
43. Oikawa M, Yoshihara T, Kaneko M. Age-related changes in articular cartilage thickness of the third metacarpal bone in the Thoroughbred. *Jpn J Vet Sci* 1989;51:839–842.
44. Yoshihara T, Kaneko M, Oikawa M, et al. An application of the image analyser to the soft radiogram of the third metacarpus in horses. *Jpn J Vet Sci* 1989;51:184–186.
45. Muller-Gerbl M, Putz R, Hodapp N, et al. Computed tomography—osteoabsorptiometry for assessing the density distribution of subchondral bone as a measure of long-term mechanical adaptation in individual joints. *Skeletal Radiol* 1989;18:507–512.
46. Eckstein F, Muller-Gerbl M, Putz R. Distribution of subchondral bone density and cartilage thickness in the human patella. *J Anat* 1992;180:425–433.
47. Les CM, Keyak JH, Stover SM, et al. Estimation of material properties in the equine metacarpus with use of quantitative computed tomography. *J Orthop Res* 1994;12:822–833.
48. Brommer H, Van Weeren PR, Brama PAJ, et al. Quantification and age-related distribution of articular cartilage degeneration of the equine fetlock joint. *Equine Vet J* 2003;35:697–701.
49. Palmer JL, Bertone AL. Joint biomechanics in the pathogenesis of traumatic arthritis. In: McIlwraith CW, Trotter GW, eds. *Joint disease in the horse*. Philadelphia: Saunders, 1996;104–119.
50. Tucker RL, Sande RD. Magnetic resonance imaging and computed tomography: evaluation of equine musculoskeletal conditions. *Vet Clin North Am Equine Pract* 2001;17:145–157.
51. Martinelli MJ, Baker GJ, Clarkson RB, et al. Magnetic resonance imaging of degenerative joint disease in a horse: a comparison to other diagnostic techniques. *Equine Vet J* 1996;28:410–415.
52. Tucker RL, Sande RD. The metacarpophalangeal (metatarsophalangeal) articulation. In: Thrall DE, ed. *Textbook of veterinary diagnostic radiology*. 4th ed. Philadelphia: WB Saunders Co, 2002;259–269.